Environ Sci Pollut Res (2015) 22:19352–19361
DOI 10.1007/s11356-015-4808-9

Microscopic biomineralization processes and Zn bioavailability: a synchrotron-based investigation of *Pistacia lentiscus* L. roots

G. De Giudici[1] · D. Medas[1] · C. Meneghini[2] · M. A. Casu[3] · A. Gianoncelli[4] · A. Iadecola[4,5] · S. Podda[6] · P. Lattanzi[1]

Received: 15 March 2015 / Accepted: 27 May 2015 / Published online: 12 June 2015

Abstract Plants growing on polluted soils need to control the bioavailability of pollutants to reduce their toxicity. This study aims to reveal processes occurring at the soil-root interface of *Pistacia lentiscus* L. growing on the highly Zn-contaminated tailings of Campo Pisano mine (SW Sardinia, Italy), in order to shed light on possible mechanisms allowing for plant adaptation. The study combines conventional X-ray diffraction (XRD) and scanning electron microscopy (SEM) with advanced synchrotron-based techniques, micro-X-ray fluorescence mapping (μ-XRF) and X-ray absorption spectroscopy (XAS). Data analysis elucidates a mechanism used by *P. lentiscus* L. as response to high Zn concentration in soil. In particular, *P. lentiscus* roots take up Al, Si and Zn from the rhizosphere minerals in order to build biomineralizations that are part of survival strategy of the species, leading to formation of a Si-Al biomineralization coating the root epidermis. XAS analysis rules out Zn binding to organic molecules and indicates that Zn coordinates Si atoms stored in root epidermis leading to the precipitation of an amorphous Zn-silicate. These findings represent a step forward in understanding biological mechanisms and the resulting behaviour of minor and trace elements during plant-soil interaction and will have significant implications for development of phytoremediation techniques.

Keywords Plant biomineralization · *Pistacia lentiscus* L. · μ-XRF · XAS · Silicon · Aluminium · Zinc · Metal bioavailability

Responsible editor: Philippe Garrigues

Electronic supplementary material The online version of this article (doi:10.1007/s11356-015-4808-9) contains supplementary material, which is available to authorized users.

✉ D. Medas
dmedas@unica.it

[1] Department of Chemical and Geological Sciences, University of Cagliari, 09127 Cagliari, Italy

[2] Science Department, University Roma Tre, 00146 Rome, Italy

[3] Institute of Translational Pharmacology, UOS of Cagliari, National Research Council, Scientific and Technological Park of Sardinia POLARIS, Pula, Italy

[4] Elettra-Sincrotrone Trieste, Basovizza, Trieste, Italy

[5] ESRF—The European Synchrotron, 71 Avenue des Martyrs, 38000 Grenoble, France

[6] CRS4—Microlab Scientific and Technological Park of Sardinia, Pula, Italy

Introduction

Survival of plant species under abiotic stresses depends primarily on the ability of the plant to react to the specific environmental stress, requiring an adaptive response (Jenks and Hasegawa 2014). This can occur by modifications of plant root architecture (Malamy 2005; Sun et al. 2008) or by modifying several aspects at cellular and metabolic levels (dos Reis et al. 2012). As pointed out in the literature, knowledge of the complex interactions ruling the rhizosphere-plant system is often empirical, and their molecular mechanisms are often only partially understood (Gardea-Torresdey et al. 2001, 2005; De Giudici et al. 2015). After the recent development, the use and evolution of microscopic and synchrotron-based probes (Majumdar et al. 2012; De Giudici et al. 2015; Medas et al. 2015) currently allow accurate investigation able to shed light on complementary aspects of physiological and molecular mechanisms.

Pistacia lentiscus is a typical plant of Mediterranean vegetation, whose ability to grow also in extreme Zn- and Pb-polluted environments is already recognized in literature (see Concas et al. 2015, and references therein). Field evidence clearly shows that this plant is able to spontaneously grow on substrates essentially consisting of residual mud accumulated during mining flotation treatment (see Fig. 2a, Campo Pisano mine, SW Sardinia, Italy). For this reason, *P. lentiscus* is being considered for phytostabilization of mine wastes (Bacchetta et al. 2012; Concas et al. 2015). As demonstrated by a fairly large body of literature, an excessive accumulation of Zn in plant tissues can cause alterations in vital growth processes (De Vos et al. 1991; Chaoui et al. 1997; Doncheva et al. 2001). However, microscopic biomineralization processes that occur at the root-soil interface and participate to the control of metal bioavailability are poorly known. The objective of this study was to determine the response of *P. lentiscus* to the highly Zn-contaminated tailings of Campo Pisano mine in order to detect possible mechanisms of plant survival strategy, which might open new perspectives in developing phytoremediation techniques. In a previous work, we found that biogeosphere processes at the interface between *Euphorbia pithyusa* roots and rhizosphere minerals result in formation of silica and Zn biomineralization, thus limiting Zn bioavailability (Medas et al. 2015). In this work, we investigate how elements such as Al, Si and Zn are taken up from the rhizosphere minerals in order to build biomineralizations that are part of survival strategy of *P. lentiscus*.

Materials and methods

Study area and samples

The Campo Pisano mine is located in the Pb-Zn-Ag Iglesiente district (SW Sardinia, Italy), one of the oldest mining districts in the world, with production dating back to pre-Roman times (Aversa et al. 2002). Campo Pisano mine was exploited until 1998. Smithsonite ($ZnCO_3$), hydrozincite ($Zn_5(CO_3)_2(OH)_6$) and hemimorphite ($Zn_4Si_2O_7(OH)_2{\cdot}(H_2O)$) are the principal Zn-bearing economic minerals of supergene ores ("calamine"). Cerussite and anglesite are also common, generally associated with nodules and lenses of residual galena (Billows 1941; Moore 1972; Stara et al. 1996; Aversa et al. 2002). The main gangue phases are calcite, quartz, iron-oxy-hydroxides and barite (Boni et al. 2003).

P. lentiscus is a shrub that grows up to 6 m tall (phanerophyte), typical component of the Mediterranean sclerophyllous shrubland, occasionally found growing on mine waste (Bacchetta et al. 2012). *P. lentiscus* investigated in this study grows on alkaline mine waste (pH ~8) highly contaminated in Zn (~14 g/kg), Pb (~4 g/kg) and Cd (~80 mg/kg; Bacchetta et al. 2015) and characterized by a low content in nutrients and C_{org} (Bacchetta et al. 2015).

Samples for this study include *P. lentiscus* roots and the soil around, in particular, (i) rhizosphere solid materials (defined here as the soil portion within 2 mm of the roots); (ii) soil (defined in this study as the soil portion beyond 2 mm and within ca. 5 cm, from the roots) and (iii) *P. lentiscus* roots collected at Campo Pisano mine, plus an additional plant harvested near the village of Fluminimaggiore (south-west Sardinia). Although this locality lies outside the mining area *stricto sensu*, it is affected by a regional geochemical anomaly with respect to Zn (De Vivo et al. 1998). Different portions of the roots were selected from *P. lentiscus* collected at the Campo Pisano mine (Table 1): (a) entire root, (b) inner part (defined in this study as the root without the epidermis) and (c) epidermis. Plants were harvested a few days before the experiments described in the following paragraphs.

Analytical methods

After plant harvesting, soil material loosely adhering to roots (for a thickness of ~2 mm) was recovered by shaking and gently wiping the roots. This material was considered to be representative of the rhizosphere surrounding the roots. Then, roots, rhizosphere materials and soil were air-dried. Approximately 200 mg of each sample was lightly ground in an agate mortar and analysed by XRD, using laboratory θ–2θ equipment (Panalytical) with Cu Kα radiation (λ= 1.54060 Å), operating at 40 kV and 40 mA, using the X′ Celerator detector.

Microscopic characteristics were investigated by scanning electron microscopy (SEM) imaging and energy dispersive spectroscopy (EDS) analysis. These were carried out using an environmental scanning electron microscope (ESEM QUANTA 200, FEI).

Different types of root sections were prepared (for details, see Medas et al. 2015) for soft X-ray microscopy combined with low-energy X-ray fluorescence (XRF) mapping analyses, that were performed at the TwinMic beamline (Kaulich et al. 2006) at ELETTRA, Trieste (Italy). The TwinMic microscope was operated in scanning transmission mode, where the monochromatized X-rays are focused on the sample through a suitable zone plate diffractive optics. While the sample is raster scan across the microprobe, a fast readout CCD camera (Andor Technology) collects the transmitted X-rays (Gianoncelli et al. 2006; Morrison et al. 2006) through an X-ray-visible light converting system, and eight SDDs (Gianoncelli et al. 2009, 2013) acquire the XRF photons emitted by the specimen. This set-up allows the simultaneous collection of X-ray absorption and phase contrast images together with elemental maps, providing simultaneous morphological and chemical information respectively.

Table 1 Root sample nomenclature, types, locations and sites

Sample	*P. lentiscus*	*P. lentiscus C. Pisano*	*P. lentiscus* inner part	*P. lentiscus* epidermis
Type	Entire root	Entire root	Inner part	Root epidermis
Location	External to the mining areas	Mine tailings	Mine tailings	Mine tailings
Site	Fluminimaggiore	Campo Pisano mine	Campo Pisano mine	Campo Pisano mine

For the present investigation, the X-ray beam energy (E= 1.985 keV) was chosen to ensure the best excitation and detection of Si, Al and Zn, with a spatial resolution (X-ray spot size) of 1 μm×1 μm as a compromise between good XRF signal and dimension of the features of interest. The XRF elemental maps were deconvoluted and analysed with PyMCA software (Sole et al. 2007).

X-ray absorption spectroscopy (XAS) experiments were carried out at the Zn K-edge (9.659 eV) at the ELETTRA-XAFS beamline (Trieste, Italy) and at the ESRF-BM23 beamline (Grenoble, France). The plant roots and rhizosphere materials were dried, ground and then pressed into solid pellets, and the Zn K-edge XAS measurements were taken via fluorescence geometry keeping the samples at the liquid nitrogen temperature. Reference materials, both inorganic and organic (see Table 2), were analysed in transmission geometry.

Standard procedures (Rehr and Albers 2000) were used for XAS data normalization and to extract the structural extended X-ray absorption fine structure (EXAFS) signal $\chi(k)$ using ESTRA code (Meneghini et al. 2012); these procedures include pre-edge linear background removal, spline modelling of bare atomic background μ_o and edge step normalization. Third degree polynomial splines (roughly spaced $\Delta k \sim 3$ Å^{-2}) were used to model the post-edge background μ_o. The photoelectron wave vector modulus $k = \sqrt{\frac{2m_e}{\hbar^2}(E-E_o)}$ (m_e being the electron mass) was calculated defining the edge energy E_o at the first inflection point (first derivative maximum) of the Zn absorption spectrum and refined during the data fitting.

Quantitative EXAFS data analysis was performed using FITEXA (Meneghini et al. 2012) to fit the raw $k\chi(k)$ spectra using the standard EXAFS formula. The multishell data refinement (Medas et al. 2014) approach is used to obtain additional details about the average local Zn structure in the samples. The relevant contributions (shells) were selected by applying statistical tests (F test) and physical constraints based on the crystallographic models (Medas et al. 2014). To evaluate the best fit quality, we report in tables also the R^2 factor:

$$R^2 = \frac{\sum_i (\chi(k_i) - \chi_{th}(k_i))^2}{\sum_i (\chi(k_i))^2}$$

quantifying the absolute misfit between experimental data and theory.[1] Here $\chi(k_i)$ and $\chi_{th}(k_i)$ are, respectively, the experimental data and the theoretical values at the point k_i.

Table 2 List of the reference compounds used for XAS analysis

Name	Formula
Willemite	Zn_2SiO_4
Hemimorphite	$Zn_4Si_2O_7(OH)_2 \cdot H_2O$
Hydrozincite	$Zn_5(CO_3)_2(OH)_6$
Smithsonite	$ZnCO_3$
Zn oxide	ZnO
Zn sulphate heptahydrate	$ZnSO_4 \cdot 7H_2O$
Zn sulphate monohydrate	$ZnSO_4 \cdot H_2O$
Zn phosphate	$Zn_3(PO_4)_2$
Zn citrate	$Zn_3(C_6H_5O_7)_2$
Zn acetate dihydrate	$Zn(O_2CCH_3)_2(H_2O)_2$
Zn acetate anhydrous	$Zn(O_2CCH_3)_2$

Results

Mineralogical and microscopic characteristics at the soil-root interface

XRPD analysis of mine residue samples (data not shown) collected at the Campo Pisano mine indicates the presence of abundant gangue minerals such as ankerite, dolomite, calcite, quartz and minor illite. Pentagonododecahedral pyrite can be recognized by SEM analysis (see Online Resource 1), together with sphalerite, barite, cerussite and smithsonite. Secondary minerals (such as gypsum, iron oxyhydroxides and Na-jarosite) form at the surfaces of mine dump as efflorescent salts.

Figure 1a–e shows diffraction peaks of some selected samples: soil (Fig. 1a), rhizosphere solid materials (Fig. 1b) and plant roots (Fig. 1c–e), all from the Campo Pisano mine. The soil sample is mainly made up of quartz, dolomite and pyrite. Rhizosphere solid materials mainly consist of quartz,

[1] Error Reporting Recommendations: A Report of the Standards and Criteria Committee, July 26, 2000—www.ixasportal.net/ixas/images/ixas_mat/Error_Reports_2000.pdf)

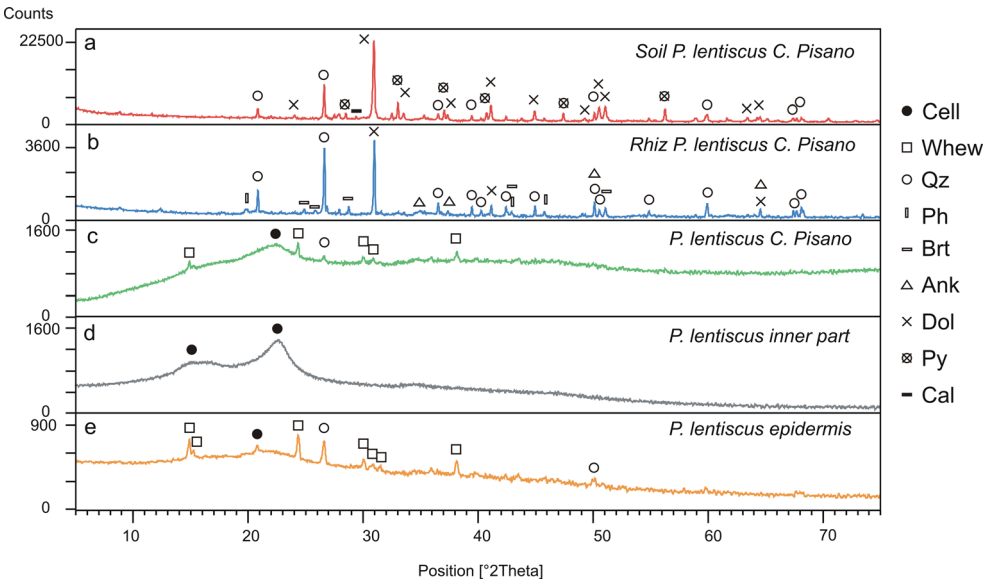

Fig. 1 XRD patterns of soil sample (**a**), rhizosphere solid materials (**b**) and plant roots (**c**–**e**) from Campo Pisano mine. Cellulose (*Cell*), whewellite (*Whew*), quartz (*Qz*), phyllosilicates (*Ph*), barite (*Brt*), ankerite (*Ank*), dolomite (*Dol*), pyrite (*Py*) and calcite (*Cal*)

dolomite, barite and ankerite. Here, pyrite peaks were not observed. XRD patterns of each portion of the *P. lentiscus* roots (entire root, inner part and epidermis, Fig. 1c–e) show the presence of amorphous cellulose, recognizable from the wide peaks at 2θ values of approximately 14.9°–16.5° and 22.8°. It is worth noting the presence of quartz and whewellite [$Ca(C_2O_4)\cdot H_2O$] in the entire root and in the epidermis sample, but these were not observed in the inner part.

Optical microscope imaging (Fig. 2b) allowed us to recognize that quartz and clay grains stick onto the surfaces of *P. lentiscus* roots. Shaking and wiping the root does not remove these phases stuck to the root surface. More in detail, SEM images of Fig. 2c–d show the narrow zone of soil immediately surrounding the root system. Raman analysis (data not shown) reveals the presence of efflorescent salts (gypsum) onto the surfaces of *P. lentiscus* roots.

To investigate biosphere-geosphere processes occurring at the soil-root interface, plant root sections were analysed by SEM. Figure 3a, d shows cross and longitudinal sections of *P. lentiscus* roots, respectively, revealing that a mineral crust precipitated at the root epidermis. SEM image at higher magnification (Fig. 3c) shows that this crust consists of a layered precipitate that follows the morphology of the root epidermis. EDS analysis (Fig. 3b_1, e_3) shows that this crust is mainly made up of Si, Al, O and C. The C signal derives from the organic matter, whereas Si and Al are related to the mineral

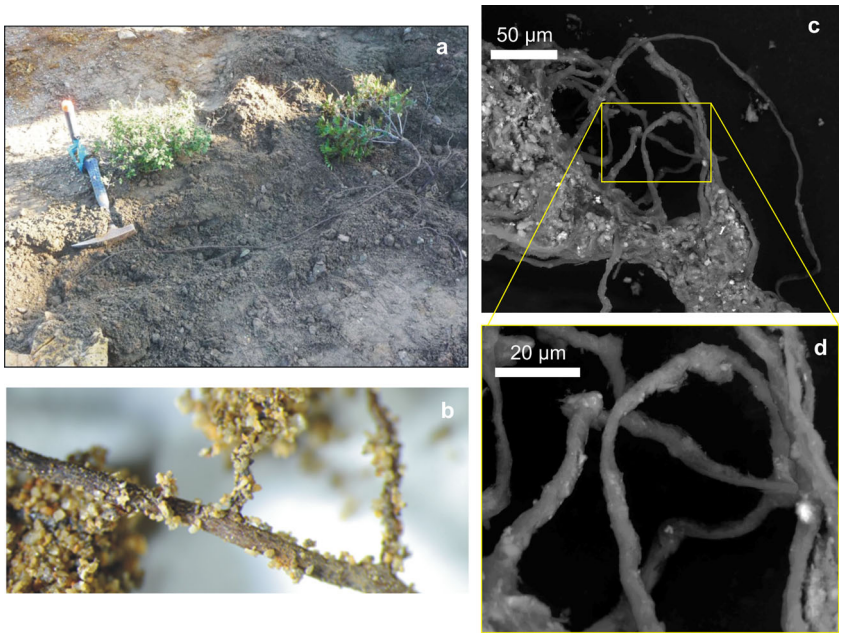

Fig. 2 *P. lentiscus* collected on the Campo Pisano mine tailings (**a**), *P. lentiscus* roots observed by optical microscope (**b**) and scanning electron microscope (**c**–**d**)

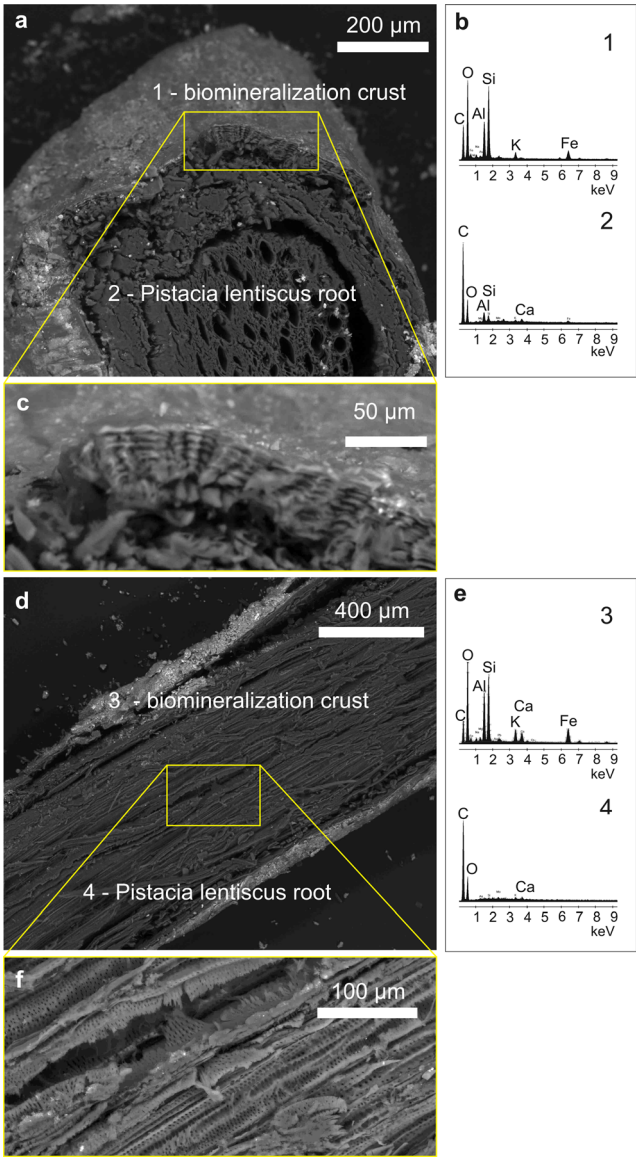

Fig. 3 Scanning electron microscopy (SEM) images of *P. lentiscus* roots (**a**, **c**, **d**, **f**) and EDS analysis (**b**, **e**). The biomineral crusts assume a layered structure

precipitate. Moving toward the inner part of the root, Si and Al signals decrease in intensity (Fig. 3b_2) and are absent in the middle part of the root (Fig. 3e_4).

These data show that the plant root activity, through processes occurring at the rhizosphere and root surfaces, drives mineral evolution and results in formation of layered coatings mainly made of Si, Al and O likely originating from biomineralization processes. These will be referred to hereafter as Si-Al biomineralization.

Distribution of Zn, Si and Al in the roots

Few micron-thick cross sections of the *P. lentiscus* roots were analysed by scanning transmission X-ray microscopy (STXM) coupled with low-energy X-ray fluorescence (LEXRF) to investigate distribution of Zn, Si and Al. Figure 4 shows four different kinds of images: (i) ordinary light stereomicroscope image, (ii) bright field (absorption) image, (iii) co-localization (Si, Al and Zn) LEXRF maps and (iv) LEXRF maps of Si, Al and Zn. These maps offer greater details than SEM imaging and analysis (see Fig. 3). Specifically, these reveal that Si and Al are mainly localized in the root epidermis forming a rim (Si-Al biomineralization), while Zn can be localized also in the inner part of the plant roots. STXM analysis suggests that when the Si-Al rim is characterized by a small thickness (~4 μm, Fig. 4b) or when this rim is not continuous (as observed in Fig. 4d), Zn penetration into the root is higher; whereas, when the Si-Al biomineralization has a higher thickness (about between 10 and 30 μm, Fig. 4c), Zn was not detected by STXM inside the root.

Zn speciation

SEM and STXM analysis show that plant root activity induces precipitation of a layered Si-Al phase at the root rim. The Si-Al biomineralization affects Zn penetration through the root epidermis suggesting that *P. lentiscus* rules Zn bioavailability by processes occurring at the root-soil surfaces. Zn K-edge XAS analysis was undertaken to evaluate Zn speciation. Figure 5 reports normalized Zn K-edge absorption spectra in the near edge (XANES) region of selected reference compounds, plant roots, soil and rhizosphere solid materials samples (see Medas et al. 2015, Fig. S5 for the complete set of the spectra of reference compounds). A qualitative XANES analysis, comparing the Zn K-edge XANES in roots with those of reference compounds, can help us to shed light about the average mineralogical environment of the absorber (Benfatto and Meneghini 2015). When compared with those of reference compounds (Fig. 5), the XANES spectral features shown by root samples are smoother and broader, pointing out a more disordered environment. Rhizosphere solid material sample spectra (Fig. 5) show features similar to those of root samples, suggesting that the most abundant Zn species in the roots is similar to that in the surrounding soil. The plant root samples depict main spectral features similar to those of hydrozincite (Fig. 5, labels A and B), with a contribution similar to that of hemimorphite/willemite (Fig. 5, labels 3 and 5). XANES spectra of root samples do not show features similar to spectra of Zn-organic compounds, as previously observed for *E. pithyusa* by Medas et al. (2015). Soil and rhizosphere samples (Fig. 5) are characterized by more pronounced spectra, pointing out a more ordered environment than in the plant roots. More in detail, the XANES features labelled as C in the Zn oxide spectrum, B in the hydrozincite spectrum and 1 and 4 in the hemimorphite/willemite spectrum are present in the *Rhiz P. lentiscus* sample. The XANES features labelled as A and B in the hydrozincite spectrum and 1 in the hemimorphite/willemite spectrum are present also in the

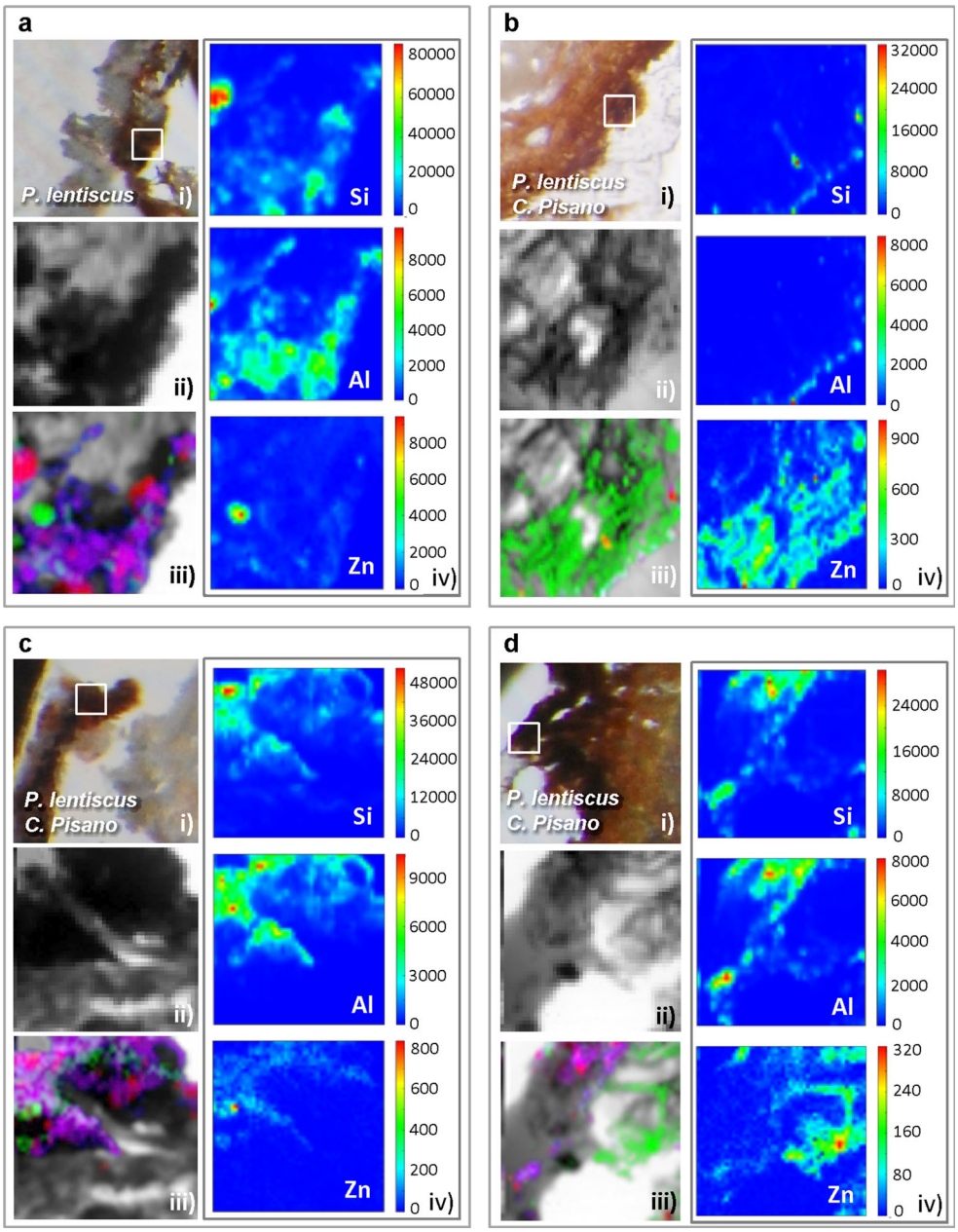

Fig. 4 Samples of *P. lentiscus*. For each sample, the following images are shown: (i) ordinary light stereomicroscope image; (ii) bright field (absorption) image; (iii) co-localization LEXRF maps (Zn—*green*, Si—*red*, Al—*blue*, Si + Al—*violet*, Si + Al + Zn—*sky blue*); and (iv) LEXRF maps of Si, Al and Zn (size 80× 80 μm^2, scan 80×80 pixels)

R. P. lentiscus C. Pisano sample. The soil collected beyond 2 mm from the plant roots (soil *P. lentiscus C. Pisano* sample) shows characteristics (labels D and E) similar to that of smithsonite.

The quantitative analysis of the EXAFS spectra was applied to achieve more detail about the Zn chemical environment. The *k*-weighted Zn EXAFS spectra $k\chi(k)$ of plant root samples are shown in Fig. 6a–b, along with the best fit curves and the Fourier transform moduli (FT). The quantitative results of EXAFS data refinement are reported in Table 3. The analysis of the EXAFS spectra collected on reference compounds (see Online Resource 2) was used to tailor the refinement procedure: The structural results of our standards are in agreement with the available literature data (ICSD 2011). Data acquisition for the *P. lentiscus* sample external to the mining area was restricted to the XANES region, because the Zn concentration in this sample is very low. Therefore, a very long acquisition time would have been necessary for the collection of data of the required statistics also in the EXAFS region.

The quantitative analysis of the EXAFS spectra measured on the entire root sample (*P. lentiscus C. Pisano*, Table 3) demonstrates Zn being approximately 5-coordinated to oxygen around R_{ZnO}=2 Å. In order to have further details, we extended the analysis to the second shell. The weak second shell at about 3 Å indicates that Zn is bound to a light element such as C, Si, P or S. The best fit was obtained by assuming the Zn second shell made by about 0.6 Si atoms. Also, a third

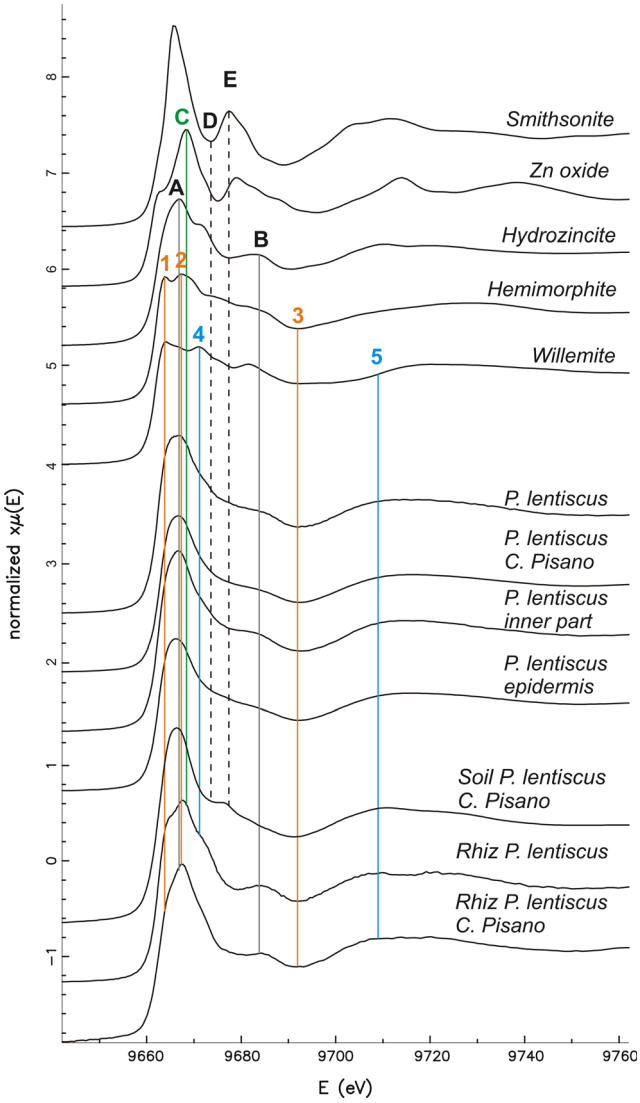

Fig. 5 Normalized absorption spectra (α) in the Zn K-edge XANES collected, from the top to the bottom, on selected reference compounds, *P. lentiscus* roots, soil sample and rhizosphere materials, vertically shifted for the sake of clarity. Similar features among root plant samples, rhizosphere materials, soil and reference compounds are highlighted

shell Zn-Zn was recognized around R_{ZnZn}=3.3 Å with a coordination number of about 5. EXAFS analysis (Table 3) from epidermis (*P. lentiscus epidermis*) and inner part of the roots (*P. lentiscus inner part*) are in agreement with results of STXM analysis. In fact EXAFS analysis reveals a second Zn-Si shell (R ~3 Å) for the epidermis and a second Zn-Zn shell (around 3.2 Å) for the inner part of the roots, where Zn-Si neighbours can be ruled out. Overall, our results indicate that ZnO5 polyhedra are not homogeneously dispersed in the plant tissues but form a Zn-rich phase in a silicate network only in the root epidermis.

Online Resource 3 shows Zn K-edge experimental $k\chi(k)$ spectra measured on the soil and rhizosphere solid material samples and their Fourier transform modulus. As observed also in the XANES region, rhizosphere samples are characterized by more ample features, pointing out a more ordered structural environment of Zn in these materials than in root samples. The analysis of the Zn EXAFS spectra of the soil and rhizosphere samples is a very difficult task because, as demonstrated by the XANES spectra analysis, these samples have a heterogeneous composition being made up of several Zn phases. Consequently, the correlation among the many parameters that should be considered would result in large error bars and poor reliability. Therefore, the quantitative analysis of the EXAFS portions of these spectra was not attempted.

Discussion and conclusion

Plants have developed different mechanisms to minimize exposure to non-essential heavy metals (Manara 2012) by ruling metal bioavailability to roots. Formation of arbuscular mycorrhiza symbioses (Turnau et al. 2010 and references therein) can play an effective role in the bioavailability of pollutants by sequestering them in extraradical hyphae (Audet and Charest 2007; Joner et al. 2000; Rufyikiri et al. 2003). Another mechanism by which plants are able to affect metal bioavailability is the secretion of root exudates, that can result in acidification, chelation, precipitation and redox reactions, or by inducing variations in physical and chemical properties of the rhizosphere (Kidd et al. 2009) and by altering the community construction and the numbers and activities of rhizospheric microbes (Dong et al. 2007). Variations in metal uptake characteristics were observed for different plant species, and for each species, metal uptake mechanisms can vary for different metals and different ranges of soil metal concentration (Baker 1981). Many plants exposed to toxic concentrations of metal ions attempt to prevent or reduce uptake by the exclusion of particular metals from the intracellular environment or the sequestration of toxic ions within compartments to isolate them from sensitive cellular components (Manara 2012).

Specifically to *P. lentiscus* investigated in this study, it grows on mine waste highly contaminated in Zn (Zn up to 1 wt%). XRD patterns of rhizosphere solid materials (Fig. 1b) do not reveal any Zn-bearing minerals, probably because these are below the instrumental detection limits; indeed, EDS analysis (data not shown) reveals the presence of Fe and Zn. More in detail, XANES analysis (Fig. 5) showed that rhizosphere solid materials have a heterogeneous composition suggesting the presence of several Zn phases (Zn oxide, hydrozincite, hemimorphite and willemite). These mineral phases seem to control Zn bioavailability in the studied soil-root system. XANES analysis (Fig. 5) showed that rhizosphere solid material samples depict main spectral features similar to those of root samples, suggesting that the most abundant Zn species in the roots is similar to that in the surrounding soil. More in

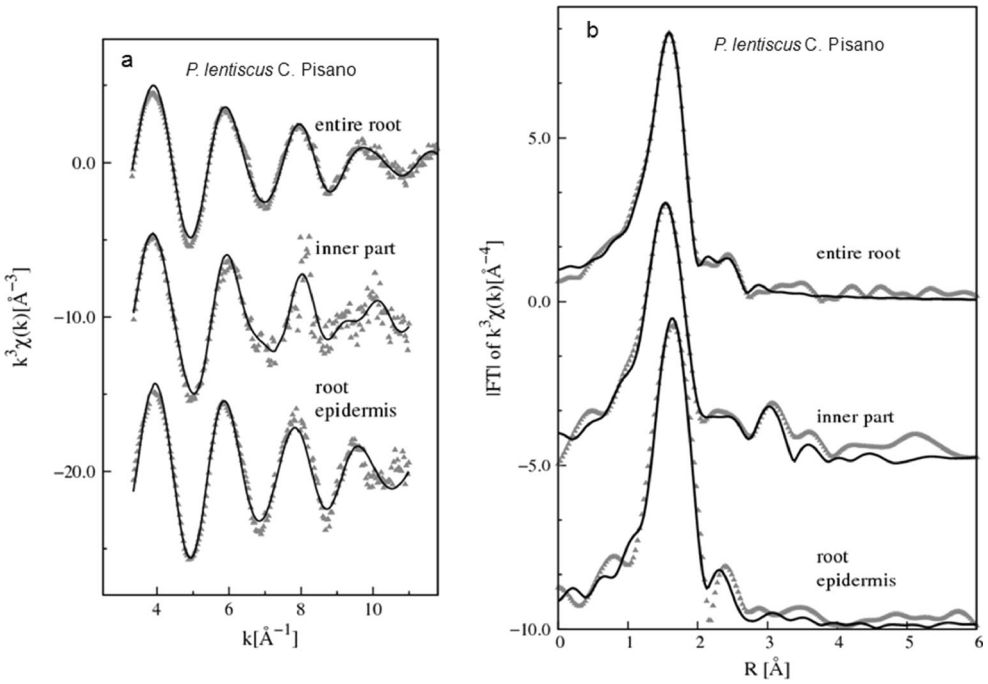

Fig. 6 Experimental data (*points*) and best fits (*full lines*) of root sample EXAFS spectra (**a**); moduli of the Fourier transforms of experimental $k\chi(k)$ and best fit curves (**b**)

detail, the LEXRF study, combined with EXAFS analysis (Fig. 6 and Table 3), rules out an organic binding complex and shows that in *P. lentiscus*, Si seems to be trapped by the root epidermis where it coordinates Zn atoms leading to the precipitation of an amorphous Zn-silicate.

Because the layered coatings were observed only at root surfaces, these biomineralizations are likely due to the interaction between root exudates, minerals and fluids and are most likely biologically induced. The physiology of roots changes with ageing of root comparts (Larcher 2003), and this could imply that biomineralization can form during a specific phase of root growth. It is worth noting that this characteristic layered biomineralization, coating the roots, was absent (unpublished results) in 3-month-old shoots of *P. lentiscus*, grown in a greenhouse on a substrate from Campo Pisano tailings (Bacchetta et al. 2015). Such a lacking of biomineralization can be due to combined effects of slow aluminosilicate weathering kinetics and difference between water abundance in greenhouse of Bacchetta et al. (2015) experiments and the drier conditions in the field.

Table 3 Fit parameters for EXAFS analysis[a]

	CN	*R* (Å)	$\sigma^2\times10^3$ (Å^2)	R^2
P. lentiscus C. Pisano				~0.03
ZnO	5.1 (3)	2.01 (2)	11 (2)	
ZnSi	0.6 (1)	2.98 (5)	6 (1)	
ZnZn	4.9 (3)	3.31 (6)	26 (4)	
P. lentiscus inner part				0.09
ZnO	5.5 (5)	1.99 (1)	12 (2)	
ZnZn	1.3 (1)	3.16 (8)	10 (1)	
P. lentiscus epidermis				0.05
ZnO	5.3 (5)	2.05 (2)	9.3 (3)	
ZnSi	0.6 (1)	3.0*	10 (2)	

[a] CN is the coordination number, *R* the interatomic distance, σ^2 the Debye-Waller factor and R^2 the best fit factor. The numbers in parentheses indicate the uncertainty on the last digit of the refined parameters. (*) denotes a fixed parameter in the fitting

The mechanisms ruling Zn uptake are still debated and depend also on Zn amount provided to the plant (see in Caldelas et al. 2011). As previously stated, in *P. lentiscus* roots, Si is mainly co-localized with Al in the epidermis forming a Si-Al biomineralization (see EDS analysis, Fig. 3, and LEXRF maps, Fig. 4). The utility of Si for plants is still under discussion, and little is known about the mechanism by which Si is deposited (Bauer et al. 2011). In our study, we observed that when the Si-Al rim has a small thickness (see Fig. 4b) or when this rim is not continuous (see Fig. 4d), Zn penetration is high. Whereas, when the Si-Al rim has a higher thickness (see Fig. 4c), as Zn inside the root is generally below the STXM detection limit, the Zn penetration is lower. Previous studies (Neumann and zur Nieden 2001; Neumann and De Figueiredo 2002) indicate that Zn binding to Si can rarely occur in plant leaves. Medas et al. (2015) proved that *E. pithyusa* can uptake Zn and Si from soil minerals and precipitates an amorphous Zn-silicate at the root rim. This rim acts as a physico-chemical barrier against organic and inorganic stresses, and its formation was interpreted as intrinsically biologically driven. A similar microscopic scale mechanism is apparently operating also for *P. lentiscus* and is in agreement with previous bulk scale investigation, showing that this species takes up Zn from soil in low amounts and

concentrates it preferentially in roots by an exclusion process (see Bacchetta et al. 2015; Concas et al. 2015). We interpreted the occurrence of Zn-silicate biomineralization and Si-Al biomineralization in the root epidermis of *P. lentiscus* as a microscopic mechanism by which this plant excludes bioavailable excess amount of Zn. Phytoremediation techniques are actually widely used for many different purposes related to management of heavy metal dispersion and pollution (see Padmavathiamma and Li 2007; van der Ent et al. 2015, and references therein). Microscopic processes occurring at the root-soil interface, such as biomineralizations, are significant for developing phytoremediation techniques (e.g. phytostabilization), because they rule element bioavailability by immobilizing metals within the plant roots. Phytoremediation techniques can benefit from future work elucidating the role of Si and Al in the plant physiology and their effect on biomineralization processes involving Zn and other metals.

Acknowledgments The study was financially supported by Regione Autonoma Sardegna (LR 7/2007 grant to P.L., Biophyto and SMERI projects) and MIUR (PRIN 2010–2011 Minerals-biosphere interaction).

References

Audet P, Charest C (2007) Dynamics of arbuscular1 mycorrhizal symbiosis in heavy metal phytoremediation: meta-analytical and conceptual perspectives. Environ Pollut 147:609–614

Aversa G, Balassone G, Boni M, Amalfitano (2002) Themineralogy of the "Calamine" ores in SW Sardinia (Italy): preliminary results. Period Mineral 71:201–218

Bacchetta G, Cao A, Cappai G, Carucci A, Casti M, Fercia ML, Lonis R, Mola F (2012) A field experiment on the use of *Pistacia lentiscus* L. and *Scrophularia canina* L. subsp. *bicolor* (Sibth. Et Sm.) Greuter for the phytoremediation of abandoned mining areas. Plant Biosyst 146:1054–1063

Bacchetta G, Cappai G, Carucci A, Tamburini E (2015) Use of native plants for the remediation of abandoned mine sites in Mediterranean semiarid environments. Bull Environ Contam Toxicol. doi:10.1007/s00128-015-1467-y

Baker AJM (1981) Accumulators and excluders strategies in the response of plants to heavy metals. J Plant Nutr 3:643–654

Bauer P, Elbaum R, Weiss IM (2011) Calcium and silicon mineralization in land plants: transport, structure and function. Plant Sci 180:746–756

Benfatto M, Meneghini C (2015) A close look into the low energy region of the XAS spectra: the XANES region. In: Mobilio S, Boscherini F, Meneghini C (eds) Synchrotron radiation, basics, methods and applications. Springer, Berlin Heidelberg, pp 213–240

Billows E (1941) I minerali della Sardegna ed i loro giacimenti: Rendiconti Università di Cagliari, p 331–335

Boni M, Gilg A, Aversa G, Balassone G (2003) The "Calamine" of SW Sardinia (Italy): geology, mineralogy and stable isotope geochemistry of a supergene Zn-mineralisation. Econ Geol 98:731–748

Caldelas C, Dong S, Araus JL, Jakob Weiss D (2011) Zinc isotopic fractionation in *Phragmites australis* in response to toxic levels of zinc. J Exp Bot 62:2169–2178

Chaoui A, Mazhoudi S, Ghorbal MH, Elferjani E (1997) Cadmium and zinc induction of lipid peroxidation and effects on antioxidant enzyme activities in bean (*Phaseolus vulgaris* L.). Plant Sci 127:139–147

Concas S, Lattanzi P, Bacchetta G, Barbafieri M, Vacca A (2015, submitted) Zn, Pb and Hg contents of *Pistacia lentiscus* L. grown on heavy-metal rich soils: implications for phytostabilization. Water Air Soil Poll

De Giudici G, Lattanzi P, Medas D (2015) Synchrotron radiation and environmental sciences synchrotron radiation. In: Mobilio S, Boscherini F, Meneghini C (eds) Synchrotron radiation, basics, methods and applications. Springer, Berlin Heidelberg, pp 661–676

De Vivo B, Boni M, Costabile S (1998) Formational anomalies versus mining pollution: geochemical risk maps of Sardinia, Italy. J Geochem Explor 64:321–337

De Vos CHR, Schat H, De Waal MAM, Voorja R, Ernst WHO (1991) Increased resistance to copper-induced damage of root cell plasmalemma in copper tolerant *Silene cucubalus*. Physiol Plant 82:523–528

Doncheva S, Stoyanova Z, Velikova V (2001) The influence of succinate on zinc toxicity of pea plant. J Plant Nutr 24:789–806

Dong J, Mao WH, Zhang GP, Cai Y (2007) Root excretion and plant tolerance to cadmium toxicity. Plant Environ J 53:193–200

dos Reis SP, Lima AM, de Souza CRBS (2012) Recent molecular advances on downstream plant responses to abiotic stress. Int J Mol Sci 13:8628–8647

Gardea-Torresdey JL, Arteaga S, Tiemann KJ, Chianelli R, Pingitore N, Mackay W (2001) Absorption of copper(II) by creosote bush (Larrea tridentata): use of atomic and x-ray absorption spectroscopy. Environ Toxicol Chem 20:2572–2579

Gardea-Torresdey JL, Videa JRP, Rosa GD, Parsons J (2005) Phytoremediation of heavy metals and study of the metal coordination by X-ray absorption spectroscopy. Coord Chem Rev 249:1797–1810

Gianoncelli A, Morrison GR, Kaulich B, Bacescu D, Kovac J (2006) A fast read-out CCD camera system for scanning X-ray microscopy. Appl Phys Lett 89:251117–251119

Gianoncelli A, Kaulich B, Alberti R, Klatka T, Longoni A, de Marco A, Marcello A, Kiskinova M (2009) Simultaneous soft X-ray transmission and emission microscopy. Nucl Instrum Methods 608:195–198

Gianoncelli A, Kourousias G, Stolfa A, Kaulich B (2013) Recent developments at the TwinMic beamline at ELETTRA: an 8 SDD detector setup for low energy X-ray. J Phys Conf Ser 425:182001

ICSD (Inorganic Crystal Structure Database) http://icsd.ill.eu/icsd/index.php, 2011

Jenks MA, Hasegawa PM (2014) Plant abiotic stress, 2nd edn. Wiley-Blackwell Publishing Inc, Oxford

Joner EJ, Briones R, Leyval C (2000) Metal-binding capacity of arbuscular mycorrhizal mycelium. Plant Soil 226:227–234

Kaulich B, Bacescu D, Susini J, David C, Di Fabrizio E, Morrison GR, Charalambous P, Thieme J, Wilhein T, Kovac J, Cocco D, Salome M, Dhez O, Weitkamp T, Cabrini S, Cojoc D, Gianoncelli A, Vogt U, Podnar M, Zangrando M, Zacchigna M, Kiskinova M (2006) Proc. 8th Int. Conf. X-ray Microscopy IPAP Conf. Series 7, 22

Kidd PS, Barceló J, Bernal MP, Navari-Izzo F, Poschenrieder C, Shilev S, Clemente R, Monterroso C (2009) Trace element behaviour at the root-soil interface: implications in phytoremediation. Environ Exp Bot 67:243–259

Larcher W (2003) Physiological plant ecology: ecophysiology and stress physiology of functional groups. Springer, Germany

Majumdar S, Peralta-Videa JR, Castillo-Michel H, Hong J, Rico CM, Gardea-Torresdey JL (2012) Applications of synchrotron μ-XRF to study the distribution of biologically important elements in different environmental matrices: a review. Anal Chim Acta 755:1–16

Malamy JE (2005) Intrinsic and environmental response pathways that regulate root system architecture. Plant Cell Environ 28:67–77

Manara A (2012) Plant responses to heavy metal toxicity. In: Antonella F (ed) Plants and Heavy Metals, SpringerBriefs in Molecular Science. Springer, Netherlands, pp 27–53

Medas D, Lattanzi P, Podda F, Meneghini C, Trapananti A, Sprocati A, Casu MA, Musu E, De Giudici G (2014) The amorphous Zn biomineralization at Naracauli stream, Sardinia: electron microscopy and X-ray absorption spectroscopy. Environ Sci Pollut R 21:6775–6782

Medas D, De Giudici G, Casu MA, Musu E, Gianoncelli A, Iadecola A, Meneghini C, Tamburini E, Sprocati AR, Turnau K, Lattanzi P (2015) Microscopic processes ruling Zn bioavailability to roots of *Euphorbia pithyusa* L. pioneer plant. Environ Sci Technol 49:1400–1408

Meneghini C, Bardelli F, Mobilio S (2012) ESTRA-FitEXA: a software package for EXAFS data analysis. Nucl Inst Methods B 285:153–157

Moore JMCM (1972) Supergene mineral deposits and physiographic development in southwest Sardinia, Italy. T I Min Metall B 71: B59–B66

Morrison GR, Gianoncelli A, Kaulich B, Bacescu D, Kovac J (2006) A fast read-out CCD system for configured-detector imaging in STXM. Conf Proc Series IPAP 7:277–379

Neumann D, De Figueiredo C (2002) A novel mechanism of silicon uptake. Protoplasma 220:59–67

Neumann D, zur Nieden U (2001) Silicon and heavy metal tolerance of higher plants. Phytochemistry 56:685–692

Padmavathiamma PK, Li LY (2007) Phytoremediation technology: hyper-accumulation metals in plants. Water Air Soil Poll 184: 105–126

Rehr JJ, Albers RC (2000) Theoretical approaches to X-ray absorption fine structure. Rev Mod Phys 72:621–654

Rufyikiri G, Thiry Y, Declerck S (2003) Contribution of hyphae and roots to uranium uptake and translocation by arbuscular mycorrhizal carrot roots under root-organ culture conditions. New Phytol 158:391–399

Sole A, Papillon E, Cotte M, Walter P, Susini J (2007) A multiplatform code for the analysis of energy-dispersive X-ray fluorescence spectra. Spectrochim Acta B 62:63–68

Stara P, Rizzo R, Tanca GA (1996) Iglesiente-Arburese, miniere e minerali. Ente Minerario Sardo I

Sun F, Zhang W, Hu H, Li B, Wang Y, Zhao Y, Li K, Liu M, Li X (2008) Salt modulates gravity signalling pathway to regulate growth direction of primary roots in Arabidopsis. Plant Physiol 146:178–188

Turnau K, Ryszka P, Wojtczak G (2010) Metal tolerant mycorrhizal plants: a review from the perspective on industrial waste in temperate region. In: Koltai H, Kapulnik Y (eds) Arbuscular mycorrhizas: physiology and function. Springer, Netherlands, pp 257–276

van der Ent A, Baker AJ, Reeves RD, Chaney RL, Anderson CW, Meech JA, Erskine PD, Simonnot MO, Vaughan J, Morel JL, Echevarria G, Fogliani B, Rongliang Q, Mulligan DR (2015) Agromining: farming for metals in the future? Environ Sci Technol. doi:10.1021/es506031u